HEALTH AND MEDICINE

Minimally instrumented SHERLOCK (miSHERLOCK) for CRISPR-based point-of-care diagnosis of SARS-CoV-2 and emerging variants

Helena de Puig[1,2,3†], Rose A. Lee[1,4,5,6†], Devora Najjar[1,2,7†], Xiao Tan[1,2,3,6,8†], Luis R. Soekensen[1,2,9], Nicolaas M. Angenent-Mari[1,2], Nina M. Donghia[1], Nicole E. Weckman[1], Audrey Ory[1,10], Carlos F. Ng[1], Peter Q. Nguyen[1], Angelo S. Mao[1,2], Thomas C. Ferrante[1], Geoffrey Lansberry[1], Hani Sallum[1], James Niemi[1], James J. Collins[1,2,3,9,10,11,12]*

The COVID-19 pandemic highlights the need for diagnostics that can be rapidly adapted and deployed in a variety of settings. Several SARS-CoV-2 variants have shown worrisome effects on vaccine and treatment efficacy, but no current point-of-care (POC) testing modality allows their specific identification. We have developed miSHERLOCK, a low-cost, CRISPR-based POC diagnostic platform that takes unprocessed patient saliva; extracts, purifies, and concentrates viral RNA; performs amplification and detection reactions; and provides fluorescent visual output with only three user actions and 1 hour from sample input to answer out. miSHERLOCK achieves highly sensitive multiplexed detection of SARS-CoV-2 and mutations associated with variants B.1.1.7, B.1.351, and P.1. Our modular system enables easy exchange of assays to address diverse user needs and can be rapidly reconfigured to detect different viruses and variants of concern. An adjunctive smartphone application enables output quantification, automated interpretation, and the possibility of remote, distributed result reporting.

INTRODUCTION

Substantial progress has been made in the use of CRISPR (clustered regularly interspaced short palindromic repeats)/Cas components of adaptive microbial immunity in molecular diagnostics (*1*–*3*). Several Cas effectors have been used as highly specific nucleic acid sensors that cause detectable collateral cleavage of engineered nucleic acid probes after target binding. SHERLOCK (specific high-sensitivity enzymatic reporter unlocking) (*4*, *5*) and DETECTR (DNA endonuclease-targeted CRISPR trans reporter) (*6*) use Cas13a or Cas12a to create ultrasensitive molecular diagnostics for a variety of targets, including infectious diseases such as Zika virus, cytomegalovirus, BK virus, and *Plasmodium* species (*4*, *7*, *8*), with simplified readouts including lateral flow assays (*5*, *7*–*9*).

Multiple CRISPR/Cas diagnostics have been created to target severe acute respiratory syndrome coronavirus 2 (SARS-CoV-2) using varied viral purification, amplification, and detection methods (*10*–*14*). However, the vast majority of workflows still require multiple liquid-handling steps and laboratory equipment such as pipettes, centrifuges, and heating blocks, as well as the technical skills for their use. Although there are several home diagnostic tests approved for use by the U.S. Food and Drug Administration (FDA), the vast majority of the tests involve self-collection followed by mailing to a central laboratory or are based on rapid antigen tests, which have been shown to be less accurate than nucleic acid–based testing with the potential for relatively high false-negative and false-positive results (*15*). There is only one FDA-approved at-home nucleic acid–based test for SARS-CoV-2, which costs $50.00 USD and requires a physician's prescription (*16*). These diagnostic methods have contributed to ongoing efforts to make SARS-CoV-2 testing as widely available as possible. However, despite these advances, all the tests described above only allow the general detection of SARS-CoV-2 and not of specific strains.

There are six general categories of SARS-CoV-2 strains (*17*), but the relationship between specific strains and mutations and changes in virulence and viral behavior are only recently being elucidated. New variants may affect transmissibility, treatment efficacy, and the degree of immunity that is generated by both natural infection and immunization (*18*). Of particular concern are variants B.1.1.7 (originally discovered in the United Kingdom), B.1.351 (originally discovered in South Africa), and P.1/B.1.1.28.1 (originally discovered in Brazil/Japan) (*19*–*21*). The N501Y spike mutation is common to all three of these variants and causes a 4- to 10-fold increased affinity to the human ACE2 receptor for SARS-CoV-2 (*22*), which is hypothesized to contribute to the observed increase in transmissibility of B.1.1.7. The B.1.351 and P.1 variants have additional receptor binding domain (RBD) mutations, such as E484K, that show markedly reduced neutralization by antibodies generated by current vaccines and by previous natural infection presumably from nonvariant SARS-CoV-2 strains (*21*, *23*–*26*).

[1]Wyss Institute for Biologically Inspired Engineering, Harvard University, Boston, MA 02115, USA. [2]Institute for Medical Engineering and Science, Department of Biological Engineering, Massachusetts Institute of Technology, Cambridge, MA 02139, USA. [3]Infectious Disease and Microbiome Program, Broad Institute of MIT and Harvard, Cambridge, MA 02142, USA. [4]Division of Infectious Diseases, Department of Pediatrics, Boston Children's Hospital, Boston, MA 02115, USA. [5]Division of Infectious Diseases, Department of Medicine, Beth Israel Deaconess Medical Center, Boston, MA 02215, USA. [6]Harvard Medical School, Boston, MA 02115, USA. [7]MIT Media Lab, Massachusetts Institute of Technology, Cambridge, MA 02139, USA. [8]Division of Gastroenterology, Massachusetts General Hospital, Boston, MA 02114, USA. [9]Abdul Latif Jameel Clinic for Machine Learning in Health, Massachusetts Institute of Technology, Cambridge, MA 02139, USA. [10]College of Arts and Sciences, Harvard University, Cambridge, MA 02138, USA. [11]Synthetic Biology Center, Massachusetts Institute of Technology, Cambridge, MA 02139, USA. [12]Harvard-MIT Program in Health Sciences and Technology, Massachusetts Institute of Technology, Cambridge, MA 02139, USA.
*Corresponding author. Email: jimjc@mit.edu
†These authors contributed equally to this work and are listed in alphabetical order.

These variants also have additional mutations in the spike N-terminal domain and appear to be resistant to several therapeutic monoclonal antibodies targeting that region (*21*). As studies advance, it is clear that the variants and their associated mutations will have a major impact on public health and the efficacy of SARS-CoV-2 control measures such as social restrictions, vaccinations, and therapies. While variant identification through specialized epidemiological sequencing centers is useful (*18*), the lack of global access to this resource and delay in result availability have hampered the tracking of and response to the spread of new SARS-CoV-2 variants. There is an urgent need for point-of-care (POC) diagnostics for SARS-CoV-2 variants. Of particular benefit would be a system that is easy to use, simple to set up, and smartphone-integrated to enable distributed, noncentralized data collection, rapid adoption, and scaled-up deployment in response to outbreaks (*18*, *27*).

Here, we describe the development of a low-cost, self-contained, POC diagnostic called miSHERLOCK (minimally instrumented SHERLOCK) that is capable of concurrent universal detection of SARS-CoV-2 as well as specific detection of the B.1.1.7, B.1.351, or P.1 variants. The miSHERLOCK platform integrates an optimized one-pot SHERLOCK reaction with an RNA paper-capture method compatible with in situ nucleic acid amplification and Cas detection. miSHERLOCK combines instrument-free, built-in sample preparation from saliva, room temperature stable reagents, battery-powered incubation, and simple visual and mobile phone–enabled output interpretation with a limit of detection (LOD) that matches U.S. Centers for Disease Control and Prevention (CDC) reverse transcription quantitative polymerase chain reaction (RT-qPCR) assays for SARS-CoV-2 of 1000 copies (cp)/ml (Fig. 1A).

Although saliva is not a commonly used clinical sample, several studies demonstrate comparable performance between saliva and nasopharyngeal samples for the detection of SARS-CoV-2 (*28*). Furthermore, in paired collection samples in hospitalized patients, salivary SARS-CoV-2 viral load has been shown to be marginally higher than nasopharyngeal swabs and positive for a greater number of days (*29*). There are also FDA-approved home-based saliva collection kits for mail-in SARS-CoV-2 diagnosis (*30*). Saliva offers the advantage of easy, instrument-free, noninvasive self-collection, which avoids dependence on limiting equipment such as swabs and transport media and decreases infectious risk to medical personnel and use of personal protective equipment during collection (*31*). However, saliva samples typically require several processing steps before use. We describe a combined filtration and concentration step from untreated saliva that is directly processed on our platform without separate processing steps and enhances our assay sensitivity.

Our platform only requires two simple user steps, is readily adjustable for additional variants or pathogen targets, and does not require transfer of amplicons, which reduces the risk of cross-contamination by lay users. We anticipate the usage of miSHERLOCK for general SARS-CoV-2 detection as well as the specific detection of N501Y and E484K mutations with the goal of locally tracking variant strains and assessing the need for variant-specific booster vaccines (*32*, *33*) such as those targeting E484K due to its effects on the efficacy of current vaccines. To showcase the flexibility of miSHERLOCK, we also demonstrate high-performance detection of the Y144del mutation.

RESULTS

Bioinformatic analysis and selection of SARS-CoV-2 target regions

A key aspect of coronavirus replication is nested transcription, which produces high levels of subgenomic RNA from the 3′ end of the SARS-CoV-2 viral genome during active infections (*34*) including the nucleoprotein (N) gene (Fig. 1B) (*35*). To identify potential targets for our assays, we performed bioinformatic analysis of conserved regions with minimal secondary structure near the 3′ end of the SARS-CoV-2 genome. We identified a region of the N gene that was highly conserved among SARS-CoV-2 sequences and that did not show homology to other coronaviruses (Fig. 1B). We designed SHERLOCK assays for this target.

SHERLOCK consists of two components: isothermal nucleic acid amplification and Cas-mediated detection. We systematically evaluated recombinase polymerase amplification (RPA) primer sets and guide RNAs (gRNAs) to determine the most sensitive combinations using commercially obtained full-length synthetic SARS-CoV-2 genomic RNA standards (Twist Bioscience MT106054.1). The best-performing N gene gRNA from a set of 30 tested showed exact target matches in 90.7% of all full-length SARS-CoV-2 sequences deposited at the U.S. National Center for Biotechnology Information (NCBI) (~43,000 genomes) (table S1). Mismatches were mostly due to a 3′ C>T single-nucleotide polymorphism (SNP) in 7.4% of sequences, which is not expected to affect Cas12a targeting because Cas12a gRNA function has been shown to be mediated primarily through 5′ interactions (*36*). The best-performing N gene RPA primers from a set of 100 pairs tested showed exact target matches in 97.4% (forward primer) and 97.0% (reverse primer) of NCBI SARS-CoV-2 genomes.

To ensure the universality of the N gene gRNA and RPA primers for SARS-CoV-2 variants, we obtained full-length high-quality sequences [>29,000 nucleotides (nt), <1% Ns, and <0.05% unique amino acid mutations not seen in other genomes] from the Global Initiative on Sharing Avian Influenza Data (GISAID) (*37*) for the B.1.1.7 (50,001 genomes), B.1.351 (577 genomes), and P.1 (78 genomes) variants and aligned as separate groups. The N gene gRNA exactly matched 99.7, 100, and 100% of B.1.1.7, B.1.351, and P.1 genomes, respectively. The N gene forward RPA primer matched 99.8, 99.5, and 100% of B.1.1.7, B.1.351, and P.1 genomes, respectively. The N gene reverse RPA primer exactly matched only 0.06% of B.1.1.7 genomes due to a C>T SNP at the +3 position from the 5′ end in 99.94% of B.1.1.7 genomes. This primer SNP is not expected to have any consequential effect on RPA amplification efficiency based on the length of RPA primers and previous studies on RPA primer design, which demonstrate a tolerance of 1- to 3-nt mismatches (*38*). The N gene reverse RPA primer exactly matched 100% of B.1.351 and P.1 genomes.

The N gene SHERLOCK assay LOD using a dilution series of heat-inactivated SARS-CoV-2 RNA [American Type Culture Collection (ATCC) VR-1986HK] spiked into water was 20,000 cp/ml with a SHERLOCK reaction time of 55 min (fig. S1). This LOD is comparable to high-performance SARS-CoV-2 RT-qPCR assays (*39*), with a faster time to result. In addition, our assay did not show any cross-reactivity against human coronavirus OC43 or human coronavirus 229E genomic RNA spiked in water (fig. S2).

SHERLOCK assays that specifically identify SARS-CoV-2 variants

To identify the B.1.1.7, B.1.351, and P.1 SARS-CoV-2 variants, we designed SHERLOCK assays that targeted a panel of key spike

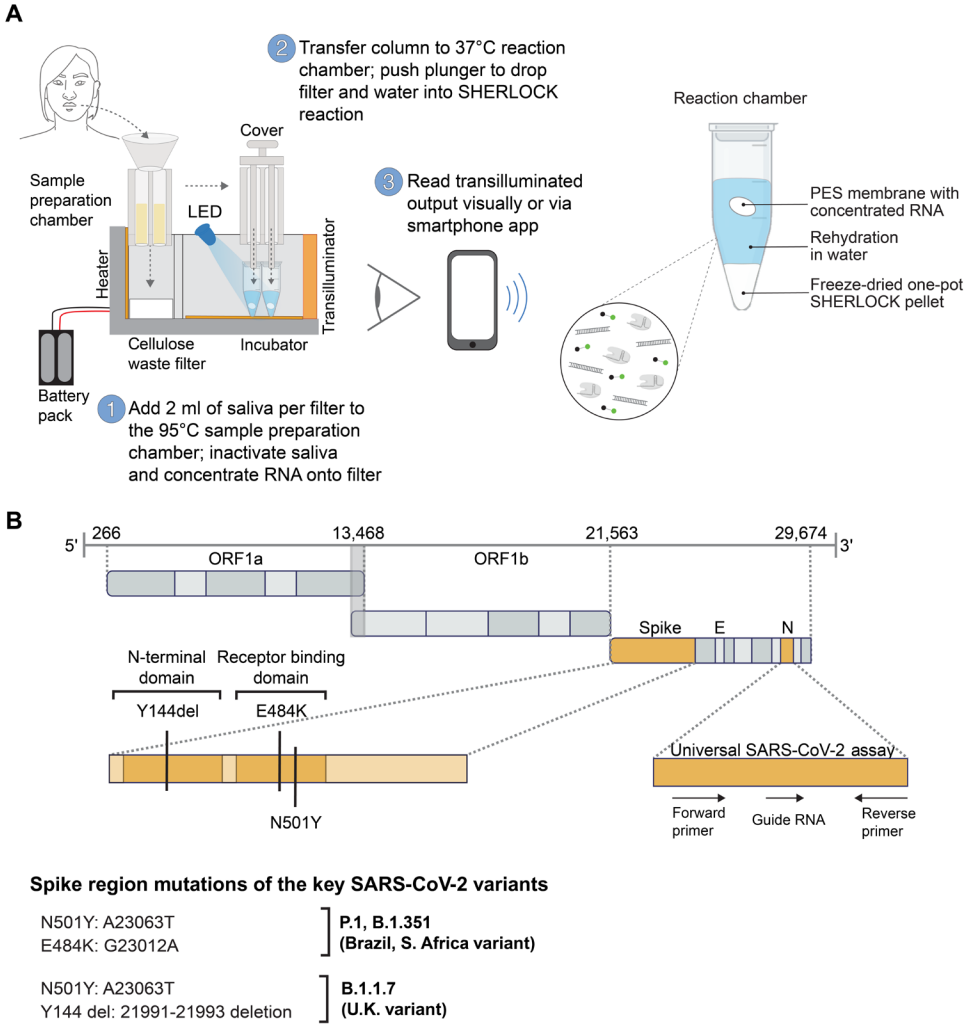

Fig. 1. Overall miSHERLOCK workflow and SARS-CoV-2 target regions. (**A**) Schematic of miSHERLOCK, which integrates instrument-free viral RNA extraction and concentration from unprocessed saliva, one-pot SHERLOCK reactions that detect SARS-CoV-2 and variants, fluorescent output, and accessory mobile phone app for automated result interpretation. Step 1: The user turns on the device and introduces 4 ml of saliva into the sample preparation chamber (2 ml per filter) and adds 40 μl of 1 M DTT and 500 mM EGTA lysis buffer. Saliva flows by gravity and capillary action through a PES membrane, which accumulates and concentrates viral RNA. Step 2: The user transfers the flow columns into the reaction chamber and depresses the plunger cover to release the PES membrane and sealed stored water into freeze-dried, one-pot SHERLOCK reaction pellets. Step 3: The user returns after 55 min and visualizes the assay directly or using a smartphone app that quantifies fluorescent output and automates result interpretation. The app may also be used for distributed remote result reporting. (**B**) SARS-CoV-2 genomic map indicating regions that are targeted in this study. The N gene target is used for a universal SARS-CoV-2 assay. SARS-CoV-2 variants are detected by targeting key mutations in the N-terminal and RBD regions of the SARS-CoV-2 spike protein, including N501Y, Y144del, and E484K.

protein mutations that are currently representative of these variants: N501Y, Y144del, and E484K (Fig. 1B). For each mutation, several gRNA sequences were designed and tested with up to 110 primer pairs to obtain the lowest LOD (fig. S3).

N501Y is a mutation in the spike RBD resulting from an A23063U SNP that is shared by the B.1.1.7, B.1.351, and P.1 SARS-CoV-2 variants. The N501Y gRNA exactly matched 99.8% of B.1.1.7 genomes, 98.8% of B.1.351 genomes, and 100% of P.1 genomes (table S1). The N501Y RPA reverse primer exactly matched 99.6, 95.3, and 100% of B.1.1.7, B.1.351, and P.1 genomes, respectively. The N501Y RPA forward primer exactly matched 98.7, 0.17, and 0% of the B.1.1.7, B.1.351, and P.1 genomes, respectively. The lack of exact matches to the B.1.351 and P.1 genomes is due to a G>A SNP at the genomic position corresponding to the +7 position from the 5′ end of the forward RPA primer in 99.3% of B.1.351 and 100% of P.1 genomes. This primer SNP is not expected to have any substantial effect on RPA amplification efficiency (*38*). Our assay targeting N501Y effectively discriminated mutant versus wild-type virus with an LOD of 100,000 cp/ml using full-length synthetic B.1.1.7 variant SARS-CoV-2 RNA spiked into water (fig. S4, A and B).

The Y144del spike mutation is a 3-nt deletion characteristic of B.1.1.7 SARS-CoV-2 variants that is not present in B.1.351 and P.1 variants. Its presence, together with N501Y, strongly suggests a B.1.1.7 variant. The Y144del gRNA showed exact matches to 98.0% of B.1.1.7 genomes and 0% of B.1.351 and P.1 genomes. The forward and reverse RPA primers exactly matched 99.7 and 99.8% of B.1.1.7 genomes, respectively (table S1). Our assay clearly distinguished between wild-type and Y144del target RNA to an LOD of 10,000 cp/ml

using full-length synthetic B.1.1.7 variant RNA diluted in water (fig. S4, C and D).

The E484K mutation is a critical spike RBD mutation present in the B.1.351, B.1.525, and P.1 SARS-CoV-2 variants, which has drawn attention. This mutation has been identified as a potential major contributor to reduced efficacy of current vaccinations and immunity resulting from natural nonvariant SARS-CoV-2 infections with demonstrably lower viral neutralizing potency from convalescent and post-vaccinated patient sera and reduced susceptibility to several therapeutic monoclonal antibodies against SARS-CoV-2 (*21*, *23*, *24*). The G23012A SNP that causes E484K also creates a new TTTN protospacer adjacent motif (PAM) site in the antisense strand that is needed for maximal Cas12a function. This is expected to allow differentiation between E484K mutant RNA and wild-type viral RNA. The E484K gRNA and forward and reverse RPA primers all exactly matched 100% of B.1.351 and P.1 genomes (table S1). The E484K gRNA and RPA primers also exactly matched to nearly 100% of B.1.1.7 genomes, but because B.1.1.7 lacks the G23012A SNP that causes E484K and therefore the TTTN PAM site, our E484K assay will have substantially reduced activation by B.1.1.7 genomes. We confirmed clear differentiation between E484K mutant and wild-type viral full-length RNA spiked into water at an LOD of 10,000 cp/ml after a reaction time of 55 min (fig. S4, E and F).

SHERLOCK assay optimization and instrument-free viral RNA capture and concentration

For POC testing targeted toward nonspecialist users, it is critical to minimize the number of user steps to reduce the likelihood of user error and contamination. We applied several engineering solutions to simplify and enhance sample preparation, one-pot SHERLOCK reactions, signal readout, and result interpretation.

SHERLOCK reaction conditions were extensively optimized by varying buffers (*6*, *7*, *13*), reverse transcriptases, and reporter concentrations to obtain the lowest LOD (fig. S5, A to C). In agreement with a previous report (*14*), we found that the addition of ribonuclease (RNase) H to the SHERLOCK reaction improved reaction kinetics and increased overall fluorescent output (fig. S5D), likely due to enhanced reverse transcriptase efficiency via degradation of inhibitory RNA:DNA hybrid intermediates.

We next adapted SHERLOCK assays for use with saliva, which has been identified as an alternative to nasopharyngeal and nasal swabs for SARS-CoV-2 diagnosis. Saliva has several advantages, including being readily available, easy to self-collect, and not requiring swabs or other collection equipment aside from a simple container, which enables mass collection (*28*, *40*). Unprocessed saliva cannot be used directly in a SHERLOCK assay without pretreatment due to salivary nucleases that hydrolyze quenched fluorescent reporters and lead to high false-positive signals (fig. S6). Unprocessed saliva is also viscous and typically requires several sample preparation steps including centrifugation and a series of manual manipulations to release genomic material from viral particles and purify them from inhibitors of nucleic acid amplification and detection reactions (*40*). POC nucleic acid tests generally require sample preparation via commercial kits (*10*, *28*, *39*, *40*), which are not suitable for applications in resource-limited settings or for at-home use by nonspecialist users.

To avoid nucleic acid purification kits that are costly, are labor-intensive, and require specialized equipment and user training, we developed a novel technique to inactivate nucleases in unprocessed saliva, lyse viral particles, and concentrate resultant nucleic acids onto a porous membrane that can be directly added to SHERLOCK detection reactions. We started by testing a variety of buffers and heating conditions (fig. S7) to inactivate nucleases and release nucleic acids from viral particles. We found that the addition of 10 mM dithiothreitol (DTT) and 5 mM EGTA followed by heating to 95°C for 3 min effectively eliminated the false-positive signal associated with salivary nucleases without inhibiting the performance of downstream SHERLOCK-based target nucleic acid detection.

Nucleic acid capture and concentration onto porous membranes compatible with in situ amplification have been described previously as a sample preparation method for nucleic acid tests (*41*–*43*). We engineered a column that collects 2 ml of user saliva (Fig. 1A) and flows the saliva to a 4-mm polyethersulfone (PES) membrane (Millipore) through gravity and capillary action from an absorbent cellulose filter applied under the membrane. The overall efficiency of nucleic acid capture is determined by the transfer rate of RNA from bulk solution to the capture matrix and the subsequent and separate binding rate of RNA to the capture matrix. We found that the highest capture efficiency is achieved by transport rates of at least 1 min/ml (fig. S8). The RNA flow rate can be finely tuned by changing the diameter of the PES membrane (fig. S9). Slowing the flow rate to 1.5 min/ml did not increase RNA recovery, but given the sharp drop-off in RNA recovery at flow rates faster than 1 min/ml, we aimed for a total flow time of 3 to 6 min to maximize RNA capture from our 2-ml sample volume, which was achieved by flowing through a 4-mm-diameter PES membrane (figs. S8 and S9). The PES membrane contains 0.22-μm pores and is functionalized with a hydrophilic surface treatment that serves as a porous matrix to capture and concentrate nucleic acids including SARS-CoV-2 RNA. The simplicity of this design allows instrument-free, intuitive liquid handling while simultaneously achieving notable specimen concentration to enable 2- to 20-fold improvement in overall signal (see below).

Construction of the miSHERLOCK integrated POC diagnostic device

We next endeavored to combine our instrument-free method of heat- and chemical-based inactivation of salivary nucleases and viral lysis and our instrument-free method of nucleic acid recovery and concentration from saliva into a low-cost, easy-to-use, integrated diagnostic device. To this end, we created miSHERLOCK, which incorporates our sample preparation methodology with SHERLOCK reactions and enables direct visual readout. In miSHERLOCK, on-device sample preparation and RNA concentration onto a PES membrane are followed by on-device physical transfer of the RNA-containing capture membrane into one-pot SHERLOCK reactions. We designed the device with two zones: a high-heat 95°C lysis area that contains an absorbent cellulose filter that wicks saliva for filtration and a low-heat 37°C reaction area that regulates SHERLOCK reaction temperature. The low-heat area contains light-emitting diodes (LEDs) and an orange acrylic optical filter for transillumination and fluorescent readout (Fig. 2, A to C). A duplexed device (for two SHERLOCK reactions) is demonstrated and validated here (Fig. 2), but the platform was designed to be scalable and modular, and we also constructed triplex (three reactions) and quadruplex (four reactions) miSHERLOCK versions (fig. S10). The heater and temperature regulator units are detachable and reusable. Our

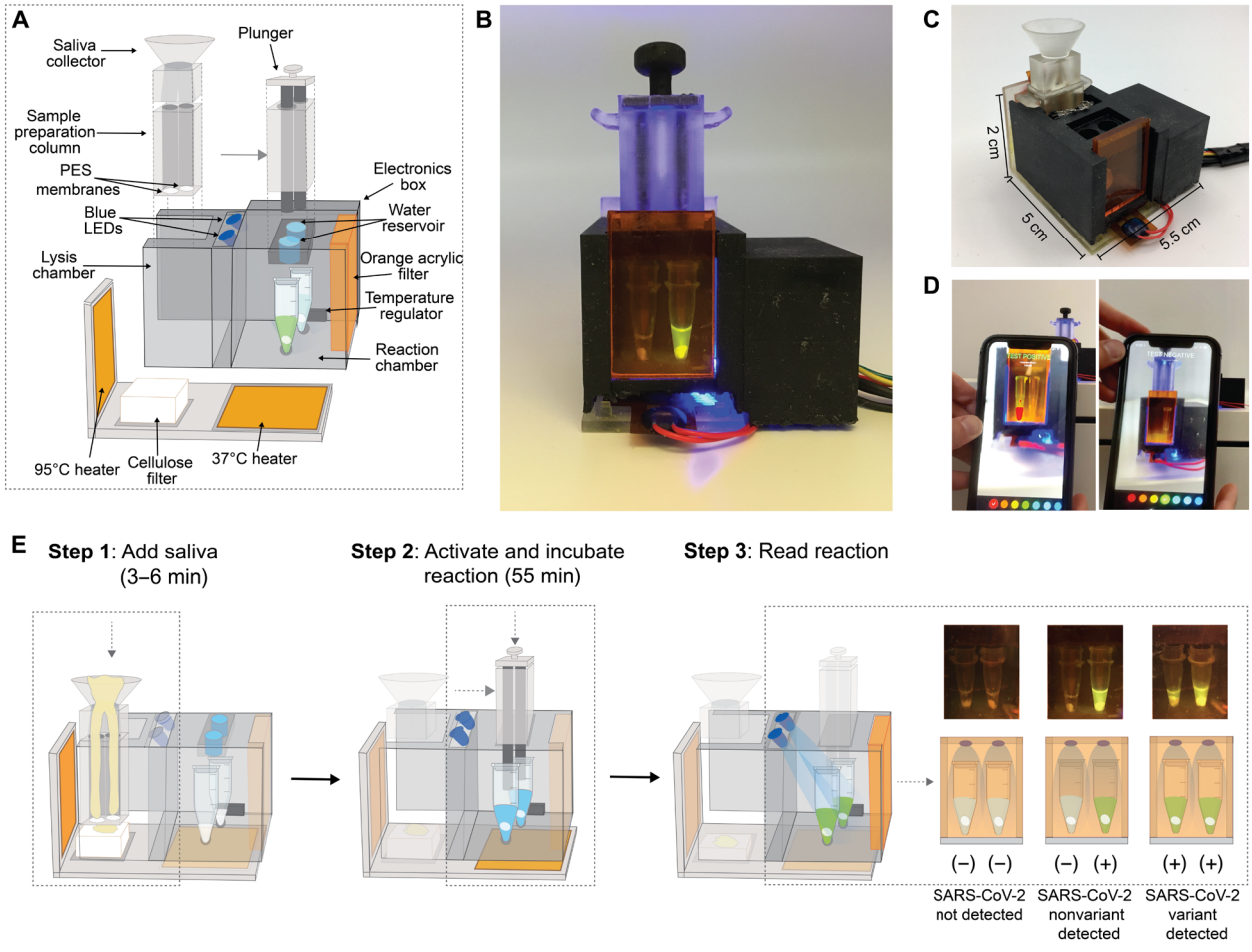

Fig. 2. miSHERLOCK device: A CRISPR-enabled POC diagnostic that integrates mechanical, electronic, biochemical, and optical components. (**A**) Exploded schematic of an integrated duplexed miSHERLOCK device with the two modules shown. (**B**) Photograph of miSHERLOCK device after reaction with positive and negative saliva samples. (**C**) Oblique view of miSHERLOCK device before use. (**D**) Adjunctive mobile phone application supports automated quantitation and result interpretation. (**E**) Workflow timing and representative examples of results. Photo credit: Devora Najjar, MIT.

diagnostic device is estimated to cost $15 (table S3), but reuse of electronics/heaters lowers costs to $6 per duplexed assay, which is mostly due to the cost of commercially obtained enzymatic components of the amplification and detection reactions (tables S3 and S4).

In the miSHERLOCK diagnostic workflow, the user introduces 2 ml of saliva into the collector, which contains preloaded lysis reagents. The user activates the heater on the device, and after 3 to 6 min, viral particles have been lysed, salivary nucleases have been inactivated, and the saliva has been wicked into the filter, leaving concentrated purified RNA on the PES membrane. The user then removes the collector and transfers the sample preparation column to the reaction chamber. The user pushes a plunger into the column, which punctures a water reservoir to rehydrate and activate the SHERLOCK reaction as well as deposits the PES membrane inside the reaction chamber. The user returns in 55 min to observe the visual fluorescence readout through the transilluminator (figs. S10 and S11 and Fig. 2E).

While SHERLOCK results are easily visually assessed by most users, we created a companion mobile phone application (app) to help provide automated quantitation and simplified interpretation of SHERLOCK results. The app uses the embedded camera in a smartphone in combination with a color segmentation algorithm to detect and quantify observed fluorescence at the end of the incubation period as compared to a fluorescence standard placed on the same reader (fig. S11). Our app quantifies the number of pixels corresponding to the selected fluorescence color to provide a simple qualitative metric of "positive" or "negative" result (Fig. 2D and movie S1). Test results can also be sent to an online database for real-time distributed disease reporting and strain tracking as required.

Evaluation of miSHERLOCK performance and validation with clinical samples

To assess the analytical sensitivity of our assays, we performed LOD studies to determine the lowest concentration at which greater than or equal to 95% of all (true positive) replicates test positive. For initial tests of miSHERLOCK performance, we used heat-inactivated SARS-CoV-2 (ATCC VR-1986HK) spiked into commercially obtained healthy human saliva to measure the LOD of our N gene universal SARS-CoV-2 assay in the integrated device. The miSHERLOCK device functioned well across a range of concentrations and showed an LOD of 1240 cp/ml [95% confidence interval (CI): 730 to 10,000] on the device (Fig. 3, A and B, and fig. S12).

To ensure that saliva samples contain enough genetic material for testing, we designed a SHERLOCK assay that targets the human RNaseP gene and validated its performance using clinical samples (fig. S13). This assay serves as a positive control for RNA extraction and reagent stability in the miSHERLOCK platform. We tested full-length synthetic RNA representative of the SARS-CoV-2 variants B.1.1.7 (Twist B.1.1.7_601443), P.1 (Twist EPI_ISL_792683), and B.1.351 (Twist EPI_ISL_678597) containing N501Y, Y144del, and E484K mutations and spiked them into commercially obtained healthy human saliva. The miSHERLOCK platform worked well across a range of concentrations and also lowered the LOD 2- to 20-fold, as compared to one-pot SHERLOCK assays performed with equivalent concentrations of synthetic full-length SARS-CoV-2 variant RNA spiked in water (fig. S4). Using the miSHERLOCK device, we determined that the LODs with observed positive rates ≥95% for the N501Y, Y144del, and E484K assays were 49,000 cp/ml (95% CI: 21,000 to 81,000), 1100 cp/ml (95% CI: 590 to 15,000), and 1200 cp/ml (95% CI: 660 to 19,000) (Fig. 3, A and D to F, and fig. S12). The differences in assay LOD were largely due to differences in RT-RPA efficiency. Given the successful integration of sample handling, salivary nuclease inactivation, viral RNA extraction, purification, concentration, and one-pot SHERLOCK in the miSHERLOCK device with improved overall signal output, we obtained clinical saliva samples from 27 RT-qPCR–positive coronavirus disease 2019 (COVID-19) patients (Boca Biolistics) to test the performance of miSHERLOCK with clinical samples. We also tested 21 healthy human saliva control samples (BioIVT). The miSHERLOCK device demonstrated 96% sensitivity and 95% specificity at a threshold of ~2000 relative fluorescence units (RFUs) (Fig. 4A) for the detection of SARS-CoV-2 in clinical saliva samples across a range of viral loads as confirmed by concurrent RT-qPCR [cycle threshold (C_T) range: 14 to 38] (Fig. 4B).

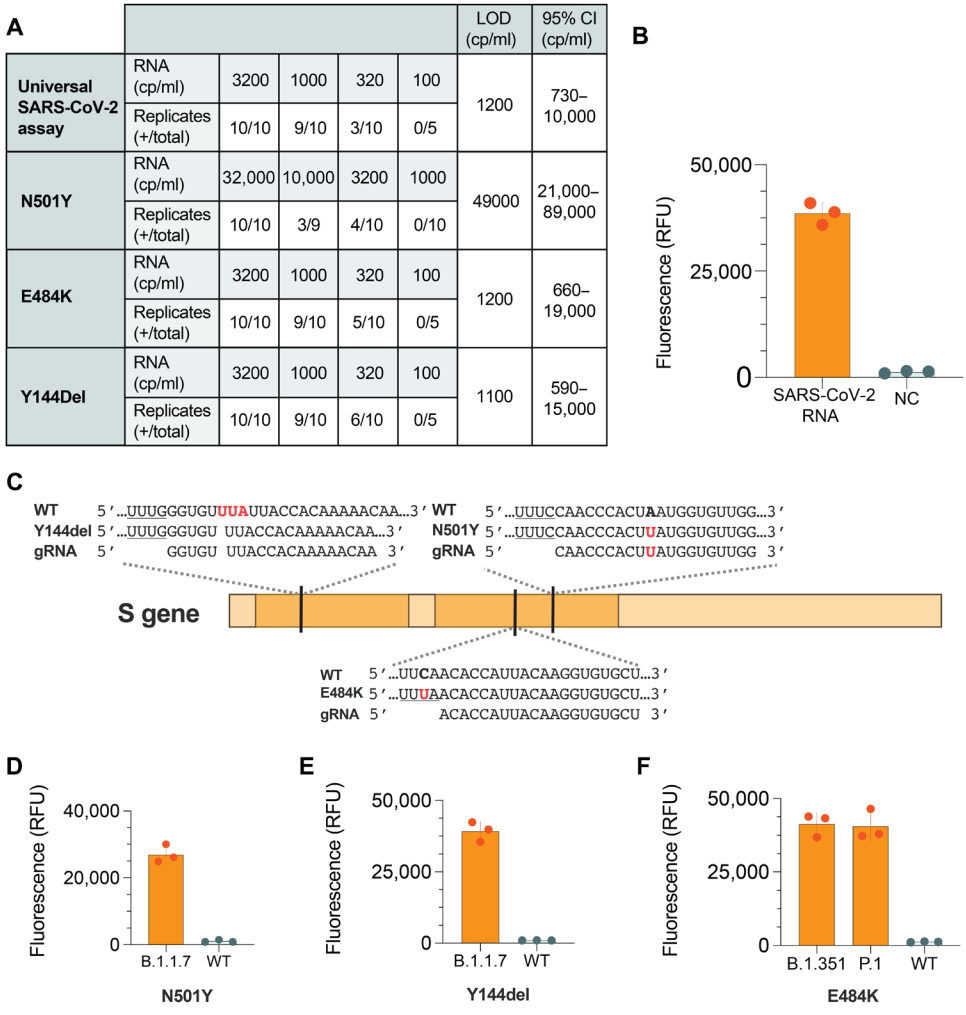

						LOD (cp/ml)	95% CI (cp/ml)
Universal SARS-CoV-2 assay	RNA (cp/ml)	3200	1000	320	100	1200	730–10,000
	Replicates (+/total)	10/10	9/10	3/10	0/5		
N501Y	RNA (cp/ml)	32,000	10,000	3200	1000	49000	21,000–89,000
	Replicates (+/total)	10/10	3/9	4/10	0/10		
E484K	RNA (cp/ml)	3200	1000	320	100	1200	660–19,000
	Replicates (+/total)	10/10	9/10	5/10	0/5		
Y144Del	RNA (cp/ml)	3200	1000	320	100	1100	590–15,000
	Replicates (+/total)	10/10	9/10	6/10	0/5		

Fig. 3. Sample processing with miSHERLOCK improves the detection of SARS-CoV-2 and variants. (**A**) Table summarizing performance near the LOD of four SARS-CoV-2 assays in the miSHERLOCK device. (**B**) Universal SARS-CoV-2 assay using 100,000 cp/ml spiked in saliva compared to healthy saliva negative control (NC). (**C**) SARS-CoV-2 spike genomic map indicating the target sequences and selected gRNA sequences that are used in this study. (**D** to **F**) Sequences of the wild type (WT) and N501Y, Y144del, and E484K mutant SARS-CoV-2 genomic regions and gRNAs. Mutation-specific gRNAs show high SHERLOCK activity when tested against full-length viral RNA containing each of the indicated mutations (orange), but only minimal SHERLOCK activation when challenged with wild-type full-length SARS-CoV-2 RNA (gray). For (D) to (F), WT control reactions were tested with WT full-length SARS-CoV-2 RNA (2,000,000 cp/ml). Error bars represent the SD of triplicate experiments.

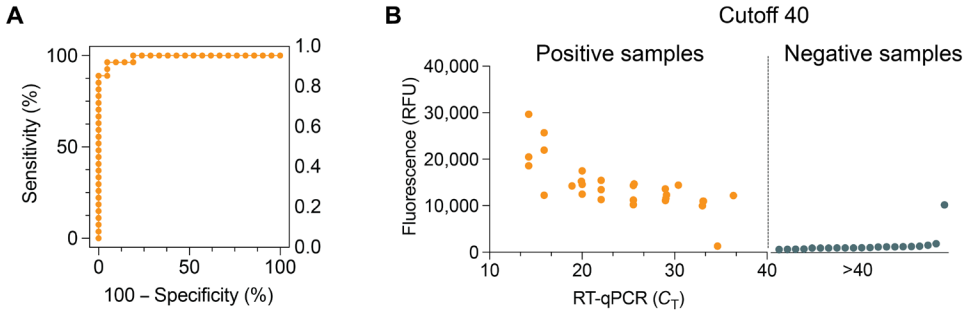

Fig. 4. miSHERLOCK accurately detects SARS-CoV-2 in clinical saliva samples. (**A**) Receiver operating characteristic curve analysis of the patient sample data collected for the universal SARS-CoV-2 assay using results from 27 RT-qPCR confirmed positive and 21 negative human saliva samples. (**B**) Clinical COVID-19 saliva sample RT-qPCR cycle threshold (C_T) plotted against fluorescent readout on miSHERLOCK demonstrates dose-dependent semiquantitative results. RT-qPCR–positive saliva samples (C_T range: 14 to 38) are plotted in orange, and RT-qPCR–negative samples ($C_T > 40$) are sorted by fluorescence and plotted in gray.

DISCUSSION

We describe the design of miSHERLOCK as a low-cost, portable, self-contained, and integrated diagnostic capable of highly sensitive universal detection of SARS-CoV-2 that equals CDC RT-qPCR performance guidelines, as well as being the only POC diagnostic capable of specific detection of SARS-CoV-2 variants. Several innovative features of our design address critical limitations of current diagnostics in the areas of assay sensitivity, ability to detect viral genomic mutations, simplicity of use, and prevention of laboratory amplicon contamination. One key feature of our design is the incorporation of a unique instrument-free method of RNA isolation from saliva that does not require laboratory equipment, yet achieves specimen filtration and concentration of sample RNA and increases assay sensitivity 2- to 20-fold. We lysed SARS-CoV-2 virions and inactivated the nucleases with a mixture of DTT/EGTA and heat. DTT and EGTA are commonly used as a reducing agent and chelator, respectively. Both can cause toxicity with excessive exposure; however, the amounts used for our tests are low. Viral RNA concentration was accomplished with a simple low-cost membrane by engineering the flow rate mediated by gravity and capillary action. Other CRISPR-based diagnostics for SARS-CoV-2 have been described but used commercial RNA extraction kits for sample preparation (*12*, *44*) or use simplified lysis that still requires several pipetting steps to perform the detection reactions (*10*, *45*).

Another innovative feature is the ability of the miSHERLOCK device to accept modular target assay components that can be easily exchanged and scaled for multiplexing as needed. Consistency of signal output interpretation is enhanced via an automated mobile phone app, which also allows distributed tracking and reporting. We demonstrate highly sensitive universal detection of SARS-CoV-2 as well as three high-performance variant diagnostic modules. Notably, these can be easily and rapidly adapted for future variants or pathogens and deployed in accordance with local conditions and diagnostic goals. The reusable heater and temperature regulator electronics minimize the cost, waste, and environmental footprint of miSHERLOCK. The device can be printed using off-the-shelf three-dimensional (3D) printers with commonly available biodegradable polylactic acid to further reduce plastic waste. Cost analysis indicates that the miSHERLOCK device has a total cost of $15, but reusing the electronics and heaters would reduce the cost to $11 per duplexed assay, mostly due to commercially obtained enzyme reagent costs that may be reduced considerably with large-scale purchasing and manufacturing (table S4). Last, amplicon contamination in nucleic acid testing is a pervasive problem that has affected several COVID-19 clinical and research laboratories (*46*). By eliminating the need to handle and transfer postamplification reactions, we substantially reduce the risk of cross-contamination, which is especially important for nonspecialist users.

Limitations of our study include the small set of clinical COVID-19 saliva samples tested due to the fact that saliva is not routinely collected in most biorepositories and was difficult to obtain within the context of a proof-of-concept exploratory study. Similarly, we were unable to test clinical samples of SARS-CoV-2 variants due to lack of availability. However, miSHERLOCK showed highly sensitive and specific detection with commercially sourced full-length variant RNA spiked into control human saliva and showed near-perfect concordance with RT-qPCR when detecting SARS-CoV-2 from clinical samples of unprocessed saliva. Our E484K variant testing relied on the difference in signal obtained in the presence of a mutated Cas12a PAM site. AsCas12a and LbaCas12a have both been shown to exhibit reduced but still present cis nucleic acid cleavage despite a TTTV to TTCV mutation, with reductions of ~80 and ~60% in cleavage efficiency in human cells, respectively (*47*). However, the effect of PAM mutations on collateral cleavage is unclear. Collateral cleavage in the absence of a TTTG PAM site has been reported for LbaCas12a (*44*), but we observed a significant difference in collateral cleavage signal between a mutated PAM site and a canonical PAM site. It is conceivable that a PAM site mutated at a single SNP (i.e., TTTA to TTCA) has a larger inhibitory effect than the complete absence of a PAM site. It is possible that, eventually, the genetic linkage between different mutations among variants would disappear as genetic drift continues. It is also possible that background mutations surrounding clinically important mutation sites may eventually make non–sequencing-based nucleic acid diagnosis of these mutations challenging. However, the number of genomes that show even a few background SNPs adjacent to the clinically relevant mutations mentioned above is extraordinarily small, and we anticipate that CRISPR-based SARS-CoV-2 mutation characterization will continue to have meaningful utility.

Given the rapid time to result of 1 hour, we believe that miSHERLOCK POC testing for SARS-CoV-2 variant strains will be highly useful for the control and management of the COVID-19 pandemic. For example, one duplex configuration could include modules for universal SARS-CoV-2 identification as well as identification of the N501Y mutation, which would detect the B.1.1.7, B.1.351, and P.1 variants. This may trigger decisions about increased

social distancing or lockdowns in response to the increased infectivity associated with N501Y variants. Another possibility is to detect the E484K mutation to guide the distribution of potential vaccine boosters (*31*, *32*) targeted to this variant due to the observed reduction in vaccine efficacy associated with the B.1.351 and P.1 strains (*19*, *21*). As ongoing clinical studies progress, mutation-specific diagnostics may also guide specific protocols in treatment and hospital infection control. For example, we anticipate that our diagnostic may be most useful at the POC in low-resource settings. While commercially prepared therapeutic cocktails of monoclonal antibodies are unlikely to be widely available in such environments because of cost, convalescent sera are expected to be more readily available and have been shown to be effective in reducing the progression to severe COVID-19 (*48*). However, current studies indicate that B.1.1.7 variants remain generally susceptible to convalescent sera, while E484K-containing variants are highly resistant to neutralization by convalescent sera (*21*). The use of our variant-focused diagnostic may therefore optimize the usage of this treatment or guide infection control policies. Although targeted to specific known mutations, miSHERLOCK may also be used as a method to triage clinical samples for further analysis with full genome sequencing for detailed epidemiological monitoring.

As new SARS-CoV-2 variants continue to evolve, the ability to identify variants and rapidly adapt diagnostics to track them will be critical to the successful treatment and containment of the ongoing COVID-19 pandemic. The streamlined workflow and flexible modular design of miSHERLOCK represent important, timely advances in the translation of CRISPR-based assays to field-applicable POC tests, particularly for low-resource settings.

MATERIALS AND METHODS

Bioinformatic analysis of SARS-CoV-2 genomes and gRNA and RPA primer design

For universal SARS-CoV-2 detection, 43,305 full-length sequences were downloaded from NCBI and aligned using MAFFT (*49*). For B.1.1.7 SARS-CoV-2 variants, 50,001 full-length high-quality (>29,000 nt, <1% Ns, and <0.05% unique amino acid mutations) genomic sequences were downloaded from GISAID (*37*) and aligned using MAFFT. For B.1.351 SARS-CoV-2 variants, 577 full-length, high-quality sequences were downloaded from GISAID and aligned using MAFFT. For P.1 SARS-CoV-2 variants, 78 full-length, high-quality sequences were downloaded from GISAID and aligned using MAFFT.

Cas12a gRNAs consist of two parts: the handle region (UAAUUUCUACUAAGUGUAGAU) that the Cas protein recognizes and binds, and a user-defined spacer region added to the 3′ end of the handle that determines the specificity to the target. Spacer regions were selected following established guidelines (*50*). For RPA amplification, we designed 10 to 21 forward and reverse RPA primers for each variant target. RPA primers for the universal SARS-CoV-2 assay (*51*) were selected after testing a range of RPA primers, including some obtained from the literature. Primers were 25 to 40 nt, and total amplicon size was 100 to 200 base pairs (bp).

Sequences were analyzed using Biopython (*52*) and JalView (*53*). Exact binding percentages of gRNAs and RPA primers for each assay to SARS-CoV-2 and variant genomes are shown in table S1. All gRNA and RPA primer sequences are listed in table S2.

Clinical samples and ethics statement

Deidentified clinical samples from the Dominican Republic were obtained from Boca Biolistics under their ethical approvals. RT-qPCR was performed by Boca Biolistics using the Perkin Elmer New Coronavirus Nucleic Acid Detection Kit. The Institutional Review Board at the Wyss Institute and Harvard University as well as the Harvard Committee on Microbiological Safety approved the use of the clinical samples in this study.

Simulated clinical samples

Simulated SARS-CoV-2 (wild type) samples were prepared by diluting commercially purchased heat-inactivated SARS-CoV-2 (ATCC VR-1986HK) quantified by qPCR into water or commercially purchased human saliva (BioIVT). Pooled saliva was prepared by mixing commercially purchased human saliva (BioIVT) from 5 to 10 different patients. Specificity targets of purified genomic RNA for human coronavirus OC43 and human coronavirus 229E were purchased from ATCC and diluted in water.

Simulated variant SARS-CoV-2 samples were prepared by spiking full-length commercially purchased variant strains for B.1.1.7 (Twist Bioscience B.1.1.7_601443), P.1 (Twist Bioscience EPI_ISL_792683), and B.1.351 (Twist Bioscience EPI_ISL_678597) in water or human saliva (BioIVT), followed by serial dilutions. Synthetic RNA of mutant target regions was also generated for initial assay characterization. To produce mutant RNA target sequences, synthetic DNA with an upstream T7 promoter sequence (5′-GAAATTAATACGACTCACTATAGGG-3′) was purchased from Integrated DNA Technologies (IDT) and in vitro transcribed to generate 150- to 500-bp RNA targets for different mutant regions using the HiScribe T7 High Yield RNA Synthesis Kit from New England Biolabs (NEB). Reactions were incubated for 16 hours at 37°C, treated with deoxyribonuclease (DNase) I (NEB), and purified using the RNA Clean & Concentrator-25 Kit (Zymo Research). RNA was quantified (ng/μl) on a NanoDrop 2000 (Thermo Fisher Scientific). The concentration of target RNA was calculated by RT-qPCR using a standard curve with quantified gene block DNA. Table S2 lists the synthetic targets and qPCR primers.

SHERLOCK RPA primer and gRNA screening

RPA primers were ordered from IDT, and the design strategy for the N and variant spike gene regions is described in Results. To synthesize gRNA, DNA sequences with an upstream T7 promoter sequence (IDT) were transcribed with the HiScribe T7 High Yield RNA Synthesis Kit (NEB). Reactions were incubated for 16 hours at 37°C, treated with DNase I (NEB), and purified using the RNA Clean & Concentrator-25 Kit (Zymo Research). We performed gRNA screens in 10 μl of volumes using 100 nM Cas12a (NEB), 200 nM gRNA, 1× NEB 2.1 buffer (NEB), 1 μM single-stranded DNA (ssDNA) fluorescent quenched reporter (56-FAM/TTATT/3IABkFQ, IDT), and 100 pM spiked target DNA standard diluted in water. Reactions were incubated at 37°C for 30 min, and fluorescence kinetics were measured using a BioTek NEO HTS plate reader (BioTek Instruments) with readings every 2 min (excitation: 485 nm; emission: 528 nm). For the SARS-CoV-2 wild-type assay, gRNAs with the highest fluorescent signal to be tested against RPA primer combinations were selected. For variant assays, we additionally tested gRNAs against 100 pM concentrations of a wild-type double-stranded DNA gene block template of the target region to ensure that Cas12a could effectively discriminate between the two targets. Best-performing

gRNAs with the highest fluorescent signal and discriminating ability were screened against multiple RPA primer sets (fig. S3). RPA screens were performed as per the manufacturer's instructions using 7.5 μl reaction volumes from the RPA Liquid Basic Kit (TwistDx) with the addition of ProtoScript Reverse Transcriptase (10 U/μl; NEB). Ten microliters of RPA primer screen reaction were added to a 1.25-μl Cas reaction with the same reaction conditions as described for the gRNA screen. Selected RPA primers and gRNAs are shown in table S2.

Sample preparation and concentration

To demonstrate paper-based RNA capture and concentration, we used an Aladdin single-syringe infusion pump (World Precision Instruments) to test different rates of low-concentration RNA flow through PES membranes (Millipore, catalog no. GPWP04700). We used an Integra surgical biopsy punch (Thermo Fisher Scientific) to create a 3-mm PES membrane disc that was compressed into the tip of a 21-gauge hypodermic needle (Becton Dickinson) and secured onto the tip of a 5-ml syringe (Becton Dickinson). The syringe was loaded onto an Aladdin infusion pump, and 2-ml volumes of SARS-CoV-2 RNA (Twist Bioscience MT106054.1) at a concentration of 500 cp/ml in water were flowed at rates of 0.25, 0.5, 1, and 1.5 min/ml through the syringe.

To optimize the flow column parameters, a 1 cm × 1 cm square of PCR sealing tape (Thermo Fisher Scientific) was cut and fitted to the bottom of the column. Different flow-through apertures were punched into the squares using Integra surgical biopsy punches at 1-, 3.5-, 5-, and 7-mm diameters, and the flow columns were loaded with PES membranes at 2-, 4-, 6-, and 8-mm diameters, respectively. One, 2, and 2.5 ml of SARS-CoV-2 RNA (Twist Bioscience) at a concentration of 1000 cp/ml in saliva were then flowed through the column. To test the sample pretreatment reagents to lyse virions and inactivate nucleases, we tried multiple detergents with and without the addition of 5 mM EGTA including 0.5% Tween 20 (Sigma-Aldrich), 1% Tween, 0.5% SDS (Sigma-Aldrich), and 1% SDS. We tested a lysis buffer composed of 4 M guanidinium thiocyanate (GITC; Sigma-Aldrich), 55 mM tris-HCl (Sigma-Aldrich), 25 mM EDTA (Sigma-Aldrich), and 3% (v/v) Triton X-100 (Sigma-Aldrich). We tested the reducing agent, DTT (Thermo Fisher Scientific), at 10, 50, and 100 mM.

One-pot lyophilized SHERLOCK assay

CRISPR-based sensor reactions were prepared using 200 nM EnGen Lba Cas12a (NEB), 400 nM gRNA, 1× NEB buffer 2.1, 430 nM each of the RPA primers (IDT), ProtoScript Reverse Transcriptase (5 U/μl; NEB), RNase H (0.05 U/μl; Ambion), 20 mM HEPES (4-(2-hydroxyethyl)-1-piperazineethanesulfonic acid) (pH 6.8) (Thomas Scientific), 60 mM NaCl (Sigma-Aldrich), 5% polyethylene glycol (Sigma-Aldrich), 1 μM fluorophore-quenched ssDNA fluorescent reporter (56-FAM/TTATT/3IABkFQ) (IDT), 14 mM magnesium acetate (TwistDx), and 1 TwistAmp Basic RPA pellet (TwistDx). Prepared sensor reactions excluding the magnesium acetate were deposited into 0.2-ml PCR tubes that were snap-frozen. Magnesium acetate was then added to the pellet, and the PCR tube was snap-frozen again before lyophilization (Labconco) for 4 to 6 hours. In-device activation of sensors was achieved by rehydration with 50 μl of water and deposition of the PES membrane with captured RNA into the reaction. SHERLOCK reactions were activated by RNA triggers diluted in water alone. Reactions proceeded for 60 to 120 min at 37°C, and fluorescent readout was measured either continuously in a BioTek NEO HTS plate reader (BioTek Instruments) or at the beginning and end of a run when reactions were performed in the miSHERLOCK device. Measurements from the miSHERLOCK device were performed via extraction of 3 μl of aliquots from the reaction tube and quantitation in the plate reader, although naked eye visual fluorescent readout was also observable in the device.

Construction of POC diagnostic device

We designed the miSHERLOCK platform using Autodesk's Fusion 360 3D CAD software. The housing and components were printed using a Formlabs Form 3 printer (Formlabs). Black resin was chosen to print the housing to minimize reflectance when reading the fluorescence assays. A 2-mm orange acrylic sheet (McMaster-Carr) was laser cut (Universal Laser Systems VLS2.30) to 2.75 cm × 2.25 cm, 2.75 cm × 3.2 cm, or 2.75 cm × 4.0 cm for the duplex, triplex, or quadruplex transilluminator filter, respectively. Double-sided tape (Scotch) was used to tightly line the water reservoir with aluminum foil (Reynolds), and 50 μl of nuclease-free water was loaded for each run. Twenty sheets of Whatman gel blotting paper GB003 (Sigma-Aldrich) were loaded into the sample preparation zone for absorption of filtered saliva. Electronic components for the polyimide heaters (Alibaba), temperature controller (DigiKey), and LED lights (Adafruit) were soldered, with heat shrink applied to all wires. Product numbers are listed in table S3. The set point for the temperature controller circuit was programmed to 37°C by selecting a 120-kilohm resistor (DigiKey) and confirmed using a Dallas DS18B20 digital temperature sensor (fig. S14). The LEDs were soldered in series with a 220-ohm resistor for the duplex and a 100-ohm resistor for the triplex, with no resistor needed for the quadruplex (DigiKey) to allow a current of 25 mA when attached to the 12-V battery source. The temperature sensor circuit and LEDs were mounted to the housing and connected to the battery pack. Folder S1 contains the STL files for our devices, fig. S15 illustrates the miSHERLOCK circuit diagrams, fig. S16 shows the electronics placement in the device, and fig. S10 shows triplexed and quadruplexed versions of the miSHERLOCK platform.

In this study, we built a mobile app using Xcode, C++, Objective-c, OpenCV 3.1, and Swift for iOS (Fig. 2D, movie S1, and folders S2 and S3). The mobile app architecture consists of a camera interface that assists in continuous capturing of fluorescence images as produced by the testing device, which are segmented on the basis of the image colors selected by the user when the user clicks over the screen showing the fluorescent regions in a standard sample. The OpenCV libraries were primarily used for image processing, which included pixel-level color detection, filtering, binarization, and masking. From a usability perspective, the software is presented as an iOS native app icon. Upon loading the app, the user can select the desired color for detection from the standard assay to then proceed toward measuring fluorescence on user-collected test tubes (movie S1). The analysis events can be screenshot and saved on the smartphone to report assay results for epidemiological purposes.

On-device miSHERLOCK reactions

We performed experiments on the miSHERLOCK platform to validate the sample preparation and one-pot lyophilized SHERLOCK reaction with patient samples. First, the 95°C heater was attached to a 24-V battery source (two 12-V batteries), and the 37°C heater, temperature regulator, and LEDs were attached to a 12-V battery source. The LEDs were inserted into their slots above the reaction chamber (fig. S16B), and the temperature regulator was inserted into the electronics box (fig. S16C). The water reservoir was covered

with a piece of foil held in place with double-sided tape and filled with 50 µl of water for reaction rehydration, the lyophilized reactions were placed within the reaction chamber, the transilluminator filter was slotted into place, the cellulose absorbent filter was placed at the bottom of the lysis chamber, and the PES filters were attached to the bottom of the sample preparation column (Fig. 2A). The sample preparation column was placed within the lysis chamber and topped with the saliva collector. For a duplexed (two-target) reaction, 4 ml of saliva, 40 µl of a 1 M DTT, and 500 mM EGTA solution were added (final concentration: 10 mM DTT and 5 mM EGTA) and then deposited into the saliva collector whereupon saliva was separated by gravity into separate sample preparation and lysis chambers. Within the lysis chamber, the saliva was inactivated by the 95°C heater, and the RNA was captured on the filter at the bottom of the column (Fig. 2E, step 1). Following the concentration, the saliva collector was removed and the sample preparation column was moved above the water reservoir. The plunger was used to deposit the filter and the water within the reservoir into the lyophilized reactions in the reaction chamber. The plunger additionally acted as a cover for the reactions and prevented evaporation during incubation (Fig. 2E, step 2). The SHERLOCK reactions were incubated for 55 to 120 min and were periodically monitored visually by observing the fluorescence through the transilluminator (Fig. 2E, step 3). Results were typically visible within 55 min of incubation and were further confirmed through the mobile app.

Data analysis

Fluorescence values are reported as absolute for all experiments used for LOD calculation. Background-subtracted fluorescence, in which the fluorescence value at the initial time point (0 min) is subtracted from the end time point (usually 60 min), is reported for initial screening experiments. Baseline initial fluorescence units differed between runs. Therefore, it was more effective to compare background-subtracted fluorescence than raw fluorescence. The relationship between the proportion of replicates testing positive and the corresponding sensitivity was examined using probit regression to estimate 95% LOD and 95% CI of each target. Image analysis of the fluorescence intensities was conducted with ImageJ (fig. S11): images of the tubes inside a miSHERLOCK device were captured with a mobile phone camera. We measured grayscale signal intensities of the areas inside the tubes and subtracted the values from background noise to obtain normalized grayscale intensities. All data were plotted, and statistical tests were performed using GraphPad Prism 8. Figures were created using BioRender or Adobe Illustrator 2020.

SUPPLEMENTARY MATERIALS

Supplementary material for this article is available at http://advances.sciencemag.org/cgi/content/full/7/32/eabh2944/DC1

View/request a protocol for this paper from *Bio-protocol*.

REFERENCES AND NOTES

1. X. Tan, J. H. Letendre, J. J. Collins, W. W. Wong, Synthetic biology in the clinic: Engineering vaccines, diagnostics, and therapeutics. *Cell* **184**, 881–898 (2021).
2. H. de Puig, I. Bosch, J. J. Collins, L. Gehrke, Point-of-care devices to detect zika and other emerging viruses. *Annu. Rev. Biomed. Eng.* **22**, 371–386 (2020).
3. R. Nouri, Z. Tang, M. Dong, T. Liu, A. Kshirsagar, W. Guan, CRISPR-based detection of SARS-CoV-2: A review from sample to result. *Biosens. Bioelectron.* **178**, 113012 (2021).
4. J. S. Gootenberg, O. O. Abudayyeh, J. W. Lee, P. Essletzbichler, A. J. Dy, J. Joung, V. Verdine, N. Donghia, N. M. Daringer, C. A. Freije, C. Myhrvold, R. P. Bhattacharyya, J. Livny, A. Regev, E. V. Koonin, D. T. Hung, P. C. Sabeti, J. J. Collins, F. Zhang, Nucleic acid detection with CRISPR-Cas13a/C2c2. *Science* **356**, 438–442 (2017).
5. J. S. Gootenberg, O. O. Abudayyeh, M. J. Kellner, J. Joung, J. J. Collins, F. Zhang, Multiplexed and portable nucleic acid detection platform with Cas13, Cas12a, and Csm6. *Science* **360**, 439–444 (2018).
6. J. S. Chen, E. Ma, L. B. Harrington, M. Da Costa, X. Tian, J. M. Palefsky, J. A. Doudna, CRISPR-Cas12a target binding unleashes indiscriminate single-stranded DNase activity. *Science* **360**, 436–439 (2018).
7. R. A. Lee, H. D. Puig, P. Q. Nguyen, N. M. Angenent-Mari, N. M. Donghia, J. P. McGee, J. D. Dvorin, C. M. Klapperich, N. R. Pollock, J. J. Collins, Ultrasensitive CRISPR-based diagnostic for field-applicable detection of Plasmodium species in symptomatic and asymptomatic malaria. *Proc. Natl. Acad. Sci. U.S.A.* **117**, 25722–25731 (2020).
8. M. M. Kaminski, M. A. Alcantar, I. T. Lape, R. Greensmith, A. C. Huske, J. A. Valeri, F. M. Marty, V. Klämbt, J. Azzi, E. Akalin, L. V. Riella, J. J. Collins, A CRISPR-based assay for the detection of opportunistic infections post-transplantation and for the monitoring of transplant rejection. *Nat. Biomed. Eng.* **4**, 601–609 (2020).
9. Y. Li, S. Li, J. Wang, G. Liu, CRISPR/Cas systems towards next-generation biosensing. *Trends Biotechnol.* **37**, 730–743 (2019).
10. J. Joung, A. Ladha, M. Saito, N.-G. Kim, A. E. Woolley, M. Segel, R. P. J. Barretto, A. Ranu, R. K. Macrae, G. Faure, E. I. Ioannidi, R. N. Krajeski, R. Bruneau, M.-L. W. Huang, X. G. Yu, J. Z. Li, B. D. Walker, D. T. Hung, A. L. Greninger, K. R. Jerome, J. S. Gootenberg, O. O. Abudayyeh, F. Zhang, Detection of SARS-CoV-2 with SHERLOCK one-pot testing. *N. Engl. J. Med.* **383**, 1492–1494 (2020).
11. Z. Ali, R. Aman, A. Mahas, G. S. Rao, M. Tehseen, T. Marsic, R. Salunke, A. K. Subudhi, S. M. Hala, S. M. Hamdan, A. Pain, F. S. Alofi, A. Alsomali, A. M. Hashem, A. Khogeer, N. A. M. Almontashiri, M. Abedalthagafi, N. Hassan, M. M. Mahfouz, iSCAN: An RT-LAMP-coupled CRISPR-Cas12 module for rapid, sensitive detection of SARS-CoV-2. *Virus Res.* **288**, 198129 (2020).
12. J. P. Broughton, X. Deng, G. Yu, C. L. Fasching, V. Servellita, J. Singh, X. Miao, J. A. Streithorst, A. Granados, A. Sotomayor-Gonzalez, K. Zorn, A. Gopez, E. Hsu, W. Gu, S. Miller, C.-Y. Pan, H. Guevara, D. A. Wadford, J. S. Chen, C. Y. Chiu, CRISPR–Cas12-based detection of SARS-CoV-2. *Nat. Biotechnol.* **38**, 870–874 (2020).
13. J. N. Rauch, E. Valois, S. C. Solley, F. Braig, R. S. Lach, M. Audouard, J. C. Ponce-Rojas, M. S. Costello, N. J. Baxter, K. S. Kosik, C. Arias, D. Acosta-Alvear, M. Z. Wilson, A scalable, easy-to-deploy, protocol for Cas13-based detection of SARS-CoV-2 genetic material. *J. Clin. Microbiol.* **59**, e02402-20 (2021).
14. J. Arizti-Sanz, C. A. Freije, A. C. Stanton, B. A. Petros, C. K. Boehm, S. Siddiqui, B. M. Shaw, G. Adams, T.-S. F. Kosoko-Thoroddsen, M. E. Kemball, J. N. Uwanibe, F. V. Ajogbasile, P. E. Eromon, R. Gross, L. Wronka, K. Caviness, L. E. Hensley, N. H. Bergman, B. L. MacInnis, C. T. Happi, J. E. Lemieux, P. C. Sabeti, C. Myhrvold, Streamlined inactivation, amplification, and Cas13-based detection of SARS-CoV-2. *Nat. Commun.* **11**, 5921 (2020).
15. U.S. Food and Drug Administration, Potential for false positive results with antigen tests for rapid detection of SARS-CoV-2—Letter to clinical laboratory staff and health care providers (2020); www.fda.gov/medical-devices/letters-health-care-providers/potential-false-positive-results-antigen-tests-rapid-detection-sars-cov-2-letter-clinical-laboratory.
16. U.S. Food and Drug Administration, Lucira COVID-19 All-In-One Test Kit Emergency Use Authorization Letter of Authorization; www.lucirahealth.com/wp-content/uploads/2020/11/Lucira-EUA-LOA.pdf.
17. H. C. Yang, C. H. Chen, J. H. Wang, H. C. Liao, C. T. Yang, C. W. Chen, Y. C. Lin, C. H. Kao, M. Y. J. Lu, J. C. Liao, Analysis of genomic distributions of SARS-CoV-2 reveals a dominant strain type with strong allelic associations. *Proc. Natl. Acad. Sci. U.S.A.* **117**, 30679–30686 (2020).
18. Public Health England, Investigation of novel SARS-COV-2 variant; https://assets.publishing.service.gov.uk/government/uploads/system/uploads/attachment_data/file/947048/Technical_Briefing_VOC_SH_NJL2_SH2.pdf.
19. CDC, Coronavirus disease 2019 (COVID-19) (Centers for Disease Control and Prevention, 2020); www.cdc.gov/coronavirus/2019-ncov/more/science-and-research/scientific-brief-emerging-variants.html.
20. Lineage B.1.525; https://cov-lineages.org/global_report_B.1.525.html#table2link.
21. P. Wang, L. Liu, S. Iketani, Y. Luo, Y. Guo, M. Wang, J. Yu, B. Zhang, P. D. Kwong, B. S. Graham, J. R. Mascola, J. Y. Chang, M. T. Yin, M. Sobieszczyk, L. Shapiro, Z. Sheng, M. S. Nair, Y. Huang, D. D. Ho, Antibody resistance of SARS-CoV-2 variants B.1.351 and B.1.1.7. *Nature* **593**, 130–135 (2021).
22. F. Tian, B. Tong, L. Sun, S. Shi, B. Zheng, Z. Wang, X. Dong, P. Zheng, Mutation N501Y in RBD of spike protein strengthens the interaction between COVID-19 and its receptor ACE2. bioRxiv 2021.02.14.431117 [**Preprint**]. 18 February 2021. https://doi.org/10.1101/2021.02.14.431117.
23. Z. Liu, L. A. VanBlargan, L.-M. Bloyet, P. W. Rothlauf, R. E. Chen, S. Stumpf, H. Zhao, J. M. Errico, E. S. Theel, M. J. Liebeskind, B. Alford, W. J. Buchser, A. H. Ellebedy, D. H. Fremont, M. S. Diamond, S. P. J. Whelan, Landscape analysis of escape variants identifies SARS-CoV-2 spike mutations that attenuate monoclonal and serum antibody neutralization. bioRxiv 2020.11.06.372037 [**Preprint**]. 8 November 2020. https://doi.org/10.1101/2020.11.06.372037.

24. C. K. Wibmer, F. Ayres, T. Hermanus, M. Madzivhandila, P. Kgagudi, B. E. Lambson, M. Vermeulen, K. van den Berg, T. Rossouw, M. Boswell, V. Ueckermann, S. Meiring, A. von Gottberg, C. Cohen, L. Morris, J. N. Bhiman, P. L. Moore, SARS-CoV-2 501Y.V2 escapes neutralization by South African COVID-19 donor plasma. *Nat. Med.* **27**, 622–625 (2021).
25. Z. Liu, L. A. VanBlargan, L.-M. Bloyet, P. W. Rothlauf, R. E. Chen, S. Stumpf, H. Zhao, J. M. Errico, E. S. Theel, M. J. Liebeskind, B. Alford, W. J. Buchser, A. H. Ellebedy, D. H. Fremont, M. S. Diamond, S. P. J. Whelan, Identification of SARS-CoV-2 spike mutations that attenuate monoclonal and serum antibody neutralization. *Cell Host Microbe* **29**, 477–488.e4 (2021).
26. A. J. Greaney, T. N. Starr, P. Gilchuk, S. J. Zost, E. Binshtein, A. N. Loes, S. K. Hilton, J. Huddleston, R. Eguia, K. H. D. Crawford, A. S. Dingens, R. S. Nargi, R. E. Sutton, N. Suryadevara, P. W. Rothlauf, Z. Liu, S. P. J. Whelan, R. H. Carnahan, J. E. Crowe, J. D. Bloom, Complete mapping of mutations to the SARS-CoV-2 spike receptor-binding domain that escape antibody recognition. *Cell Host Microbe* **29**, 44–57.e9 (2021).
27. B. Udugama, P. Kadhiresan, H. N. Kozlowski, A. Malekjahani, M. Osborne, V. Y. C. Li, H. Chen, S. Mubareka, J. B. Gubbay, W. C. W. Chan, Diagnosing COVID-19: The disease and tools for detection. *ACS Nano* **14**, 3822–3835 (2020).
28. R. A. Lee, J. C. Herigon, A. Benedetti, N. R. Pollock, C. M. Denkinger, Performance of saliva, oropharyngeal swabs, and nasal swabs for SARS-CoV-2 molecular detection: A systematic review and meta-analysis. *J. Clin. Microbiol.* **59**, e02881-20 (2021).
29. A. L. Wyllie, J. Fournier, A. Casanovas-Massana, M. Campbell, M. Tokuyama, P. Vijayakumar, J. L. Warren, B. Gen, M. C. Muenker, A. J. Moore, C. B. F. Vogels, M. E. Petrone, I. M. Ott, P. Lu, A. Venkataraman, A. Lu-Culligan, J. Klein, R. Earnest, M. Simonov, R. Datta, R. Handoko, N. Naushad, L. R. Sewanan, J. Valdez, E. B. White, S. Lapidus, C. C. Kalinich, X. Jiang, D. J. Kim, E. Kudo, M. Linehan, T. Mao, M. Moriyama, J. E. Oh, A. Park, J. Silva, E. Song, T. Takahashi, M. Taura, O. E. Weizman, P. Wong, Y. Yang, S. Bermejo, C. D. Odio, S. B. Omer, C. S. Dela Cruz, S. Farhadian, R. A. Martinello, A. Iwasaki, N. D. Grubaugh, A. L. Ko, Saliva or nasopharyngeal swab specimens for detection of SARS-CoV-2. *N. Engl. J. Med.* **383**, 1283–1286 (2020).
30. P23, P23 At-Home COVID-19 Test Collection Kit—Instructions for Use (2021); www.fda.gov/media/140087/download.
31. H. C. Ates, A. Brunauer, F. von Stetten, G. A. Urban, F. Güder, A. Merkoçi, S. M. Früh, C. Dincer, Integrated devices for non-invasive diagnostics. *Adv. Funct. Mater.* **31**, 2010388 (2021).
32. Moderna Inc.,Moderna announces it has shipped variant-specific vaccine candidate, mRNA-1273.351, to NIH for clinical study; https://investors.modernatx.com/news-releases/news-release-details/moderna-announces-it-has-shipped-variant-specific-vaccine/.
33. A. Lardieri, "Pfizer, BioNTech test third "booster" shot against coronavirus variants," *US News & World Report*, 25 February 2021; www.usnews.com/news/health-news/articles/2021-02-25/pfizer-biontech-test-third-booster-shot-against-coronavirus-variants.
34. P. V'kovski, A. Kratzel, S. Steiner, H. Stalder, V. Thiel, Coronavirus biology and replication: Implications for SARS-CoV-2. *Nat. Rev. Microbiol.* **19**, 155–170 (2021).
35. Y. Finkel, O. Mizrahi, A. Nachshon, S. Weingarten-Gabbay, D. Morgenstern, Y. Yahalom-Ronen, H. Tamir, H. Achdout, D. Stein, O. Israeli, A. Beth-Din, S. Melamed, S. Weiss, T. Israely, N. Paran, M. Schwartz, N. Stern-Ginossar, The coding capacity of SARS-CoV-2. *Nature* **589**, 125–130 (2021).
36. D. C. Swarts, J. van der Oost, M. Jinek, Structural basis for guide RNA processing and seed-dependent DNA targeting and cleavage by CRISPR-Cas12a. *Mol. Cell.* **66**, 221–233.e4 (2017).
37. S. Elbe, G. Buckland-Merrett, Data, disease and diplomacy: GISAID's innovative contribution to global health. *Global Chall.* **1**, 33–46 (2017).
38. X. Liu, Q. Yan, J. Huang, J. Chen, Z. Guo, Z. Liu, L. Cai, R. Li, Y. Wang, G. Yang, Q. Lan, Influence of design probe and sequence mismatches on the efficiency of fluorescent RPA. *World J. Microbiol. Biotechnol.* **35**, 95 (2019).
39. CDC 2019-nCoV Real-Time RT-PCR Diagnostic Panel (CDC)—Manufacturer Instructions/Package Insert | FDA; www.fda.gov/media/134922/download.
40. B. M. Berenger, J. M. Conly, K. Fonseca, J. Hu, T. Louie, A. R. Schneider, T. Singh, W. Stokes, L. Ward, N. Zelyas, Saliva collected in universal transport media is an effective, simple and high-volume amenable method to detect SARS-CoV-2. *Clin. Microbiol. Infect.* **27**, 656–657 (2020).
41. J. C. Linnes, N. M. Rodriguez, L. Liu, C. M. Klapperich, Polyethersulfone improves isothermal nucleic acid amplification compared to current paper-based diagnostics. *Biomed. Microdevices* **18**, 30 (2016).
42. N. M. Rodriguez, J. C. Linnes, A. Fan, C. K. Ellenson, N. R. Pollock, C. M. Klapperich, Paper-based RNA extraction, in situ isothermal amplification, and lateral flow detection for low-cost, rapid diagnosis of influenza a (H1N1) from clinical specimens. *Anal. Chem.* **87**, 7872–7879 (2015).
43. T. S. Schlappi, S. E. McCalla, N. G. Schoepp, R. F. Ismagilov, Flow-through capture and in situ amplification can enable rapid detection of a few single molecules of nucleic acids from several milliliters of solution. *Anal. Chem.* **88**, 7647–7653 (2016).
44. X. Ding, K. Yin, Z. Li, R. V. Lalla, E. Ballesteros, M. M. Sfeir, C. Liu, Ultrasensitive and visual detection of SARS-CoV-2 using all-in-one dual CRISPR-Cas12a assay. *Nat. Commun.* **11**, 4711 (2020).
45. B. Ning, T. Yu, S. Zhang, Z. Huang, D. Tian, Z. Lin, A. Niu, N. Golden, K. Hensley, B. Threeton, C. J. Lyon, X. M. Yin, C. J. Roy, N. S. Saba, J. Rappaport, Q. Wei, T. Y. Hu, A smartphone-read ultrasensitive and quantitative saliva test for COVID-19. *Sci. Adv.* **7**, eabe3703 (2021).
46. L. R. Robinson-McCarthy, A. J. Mijalis, G. T. Filsinger, H. de Puig, N. M. Donghia, T. E. Schaus, R. A. Rasmussen, R. Ferreira, J. E. Lunshof, G. Chao, D. Ter-Ovanesyan, O. Dodd, E. Kuru, A. M. Sesay, J. Rainbow, A. C. Pawlowski, T. M. Wannier, P. Yin, J. J. Collins, D. E. Ingber, G. M. Church, J. M. Tam, Anomalous COVID-19 tests hinder researchers. *Science* **371**, 244–245 (2021).
47. P. Chen, J. Zhou, Y. Wan, H. Liu, Y. Li, Z. Liu, H. Wang, J. Lei, K. Zhao, Y. Zhang, Y. Wang, X. Zhang, L. Yin, A Cas12a ortholog with stringent PAM recognition followed by low off-target editing rates for genome editing. *Genome Biol.* **21**, 78 (2020).
48. R. Libster, G. Pérez Marc, D. Wappner, S. Coviello, A. Bianchi, V. Braem, I. Esteban, M. T. Caballero, C. Wood, M. Berrueta, A. Rondan, G. Lescano, P. Cruz, Y. Ritou, V. Fernández Viña, D. Álvarez Paggi, S. Esperante, A. Ferreti, G. Ofman, A. Ciganda, R. Rodriguez, J. Lantos, R. Valentini, N. Itcovici, A. Hintze, M. L. Oyarvide, C. Etchegaray, A. Neira, I. Name, J. Alfonso, R. López Castelo, G. Caruso, S. Rapelius, F. Alvez, F. Etchenique, F. Dimase, D. Alvarez, S. S. Aranda, C. Sánchez Yanotti, J. De Luca, S. Jares Baglivo, S. Laudanno, F. Nowogrodzki, R. Larrea, M. Silveyra, G. Leberzstein, A. Debonis, J. Molinos, M. González, E. Perez, N. Kreplak, S. Pastor Argüello, L. Gibbons, F. Althabe, E. Bergel, F. P. Polack; Fundación INFANT–COVID-19 Group, Early high-titer plasma therapy to prevent severe COVID-19 in older adults. *N. Engl. J. Med.* **384**, 610–618 (2021).
49. K. Katoh, D. M. Standley, MAFFT multiple sequence alignment software version 7: Improvements in performance and usability. *Mol. Biol. Evol.* **30**, 772–780 (2013).
50. R. V. Gayet, H. de Puig, M. A. English, L. R. Soenksen, P. Q. Nguyen, A. S. Mao, N. M. Angenent-Mari, J. J. Collins, Creating CRISPR-responsive smart materials for diagnostics and programmable cargo release. *Nat. Protoc.* **15**, 3030–3063 (2020).
51. M. Patchsung, K. Jantarug, A. Pattama, K. Aphicho, S. Suraritdechachai, P. Meesawat, K. Sappakhaw, N. Leelahakorn, T. Ruenkam, T. Wongsatit, N. Athipanyasilp, B. Eiamthong, B. Lakkanasirorat, T. Phoodokmai, N. Niljianskul, D. Pakotiprapha, S. Chanarat, A. Homchan, R. Tinikul, P. Kamutira, K. Phiwkaow, S. Soithongcharoen, C. Kantiwiriyawanitch, V. Pongsupasa, D. Trisrivirat, J. Jaroensuk, T. Wongnate, S. Maenpuen, P. Chaiyen, S. Kamnerdnakta, J. Swangsri, S. Chuthapisith, Y. Sirivatanauksorn, C. Chaimayo, R. Sutthent, W. Kantakamalakul, J. Joung, A. Ladha, X. Jin, J. S. Gootenberg, O. O. Abudayyeh, F. Zhang, N. Horthongkham, C. Uttamapinant, Clinical validation of a Cas13-based assay for the detection of SARS-CoV-2 RNA. *Nature. Biomed. Eng.* **4**, 1140–1149 (2020).
52. P. J. A. Cock, T. Antao, J. T. Chang, B. A. Chapman, C. J. Cox, A. Dalke, I. Friedberg, T. Hamelryck, F. Kauff, B. Wilczynski, M. J. L. de Hoon, Biopython: Freely available Python tools for computational molecular biology and bioinformatics. *Bioinformatics* **25**, 1422–1423 (2009).
53. A. M. Waterhouse, J. B. Procter, D. M. A. Martin, M. Clamp, G. J. Barton, Jalview Version 2—A multiple sequence alignment editor and analysis workbench. *Bioinformatics* **25**, 1189–1191 (2009).

Acknowledgments: We thank M. A. English for helpful discussions and advice. **Funding:** This work was supported by the Paul G. Allen Frontiers Group, and the Wyss Institute for Biologically Inspired Engineering, Harvard University. H.d.P. was supported by the Harvard University Center for AIDS Research (CFAR), an NIH-funded program (P30 AI060354), which is supported by the following NIH co-funding and participating Institutes and Centers: NIAID, NCI, NICHD, NIDCR, NHLBI, NIDA, NIMH, NIA, NIDDK, NINR, NIMHD, FIC, and OAR. R.A.L. was supported by the Burroughs-Wellcome American Society of Tropical Medicine and Hygiene postdoctoral fellowship. X.T. was supported by an American Gastroenterological Association Takeda Pharmaceutical Research Scholar Award in Inflammatory Bowel Disease. N.M.A.-M. was supported by an MIT-TATA Center fellowship 2748460. **Author contributions:** H.d.P., R.A.L., D.N., and X.T. designed and performed experiments, analyzed the data, and wrote the manuscript. L.R.S., N.M.A.-M., N.M.D., N.E.W., C.F.N., P.Q.N., A.O., A.S.M., T.C.F., G.L., H.S., and J.N. performed experiments and edited the manuscript. J.J.C. directed overall research and edited the manuscript. **Competing interests:** J.J.C. is a cofounder and director of Sherlock Biosciences. N.E.W. is a cofounder and consults for 52 North Health Ltd. All other authors declare no competing interests. **Data and materials availability:** All data needed to evaluate the conclusions in the paper are present in the paper and/or the Supplementary Materials.

Submitted 1 March 2021
Accepted 17 June 2021
Published 6 August 2021
10.1126/sciadv.abh2944

Citation: H. de Puig, R. A. Lee, D. Najjar, X. Tan, L. R. Soekensen, N. M. Angenent-Mari, N. M. Donghia, N. E. Weckman, A. Ory, C. F. Ng, P. Q. Nguyen, A. S. Mao, T. C. Ferrante, G. Lansberry, H. Sallum, J. Niemi, J. J. Collins, Minimally instrumented SHERLOCK (miSHERLOCK) for CRISPR-based point-of-care diagnosis of SARS-CoV-2 and emerging variants. *Sci. Adv.* **7**, eabh2944 (2021).

Minimally instrumented SHERLOCK (miSHERLOCK) for CRISPR-based point-of-care diagnosis of SARS-CoV-2 and emerging variants

Helena de Puig, Rose A. Lee, Devora Najjar, Xiao Tan, Luis R. Soekensen, Nicolaas M. Angenent-Mari, Nina M. Donghia, Nicole E. Weckman, Audrey Ory, Carlos F. Ng, Peter Q. Nguyen, Angelo S. Mao, Thomas C. Ferrante, Geoffrey Lansberry, Hani Sallum, James Niemi and James J. Collins

Sci Adv **7** (32), eabh2944.
DOI: 10.1126/sciadv.abh2944